

# Flight testing of terrain-relative navigation and large-divert guidance on a VTVL rocket

Nikolas Trawny, Joel Benito, Brent Tweddle, Charles F. Bergh,  
Garen Khanoyan, Geoffrey M. Vaughan, Jason X. Zheng, Carlos Y. Villalpando,  
Yang Cheng, Daniel P. Scharf, Charles D. Fisher, Phoebe M. Sulzen,  
James F. Montgomery, Andrew E. Johnson, and MiMi Aung

*Jet Propulsion Laboratory, California Institute of Technology, Pasadena, CA 91109*

Martin W. Regehr\*

*Christie, Parker & Hale, LLP, 655 North Central Avenue, Suite 2300, Glendale, California 91203*

Daniel Dueri and Behçet Açıkmese

*University of Texas at Austin, Aerospace Engineering and Engineering Mechanics, Austin, TX 78712*

David Masten, Travis O’Neal and Scott Nietfeld

*Masten Space Systems, 1570 Sabovich St, Mojave, CA 93501*

Since 2011, the Autonomous Descent and Ascent Powered-Flight Testbed (ADAPT) has been used to demonstrate advanced descent and landing technologies onboard the Masten Space Systems (MSS) Xombie vertical-takeoff, vertical-landing suborbital rocket. The current instantiation of ADAPT is a stand-alone payload comprising sensing and avionics for terrain-relative navigation and fuel-optimal onboard planning of large divert trajectories, thus providing complete pin-point landing capabilities needed for planetary landers. To this end, ADAPT combines two technologies developed at JPL, the Lander Vision System (LVS), and the Guidance for Fuel Optimal Large Diverts (G-FOLD) software. This paper describes the integration and testing of LVS and G-FOLD in the ADAPT payload, culminating in two successful free flight demonstrations on the Xombie vehicle conducted in December 2014.

## I. Introduction

TO date, robotic planetary landers have landed without absolute position information, resulting in km-level landing ellipses. This precludes landing close to hazardous but scientifically interesting landing sites or pre-positioned surface assets, thus eliminating some landing sites or resulting in long drive-to times. The desire for safer and more accurate landing systems to enable “landing on science” has resulted in significant research and development of pin-point landing technologies, specifically terrain-relative navigation (TRN) and large divert guidance algorithms. Using these technologies, future landers will recognize landmarks and compute their positions relative to a stored map, which can then be used by large divert guidance to guide the lander to a nearby safe landing site (multi-point landing) or to the center of the landing ellipse (pin-point landing), see Fig. 1.

The Autonomous Descent and Ascent Powered-Flight Testbed (ADAPT) was designed to demonstrate such next generation guidance, navigation, and control technologies, running closed-loop on a free-flying vehicle, in dynamic conditions emulating the final descent through touchdown during a Mars landing.<sup>2</sup> Leveraging commercial rocket-powered flight test capabilities available through a partnership with Masten Space Systems and the NASA Flight Opportunities Program, ADAPT enables rapid, cost-efficient technology

---

\*Work carried out while employed at JPL

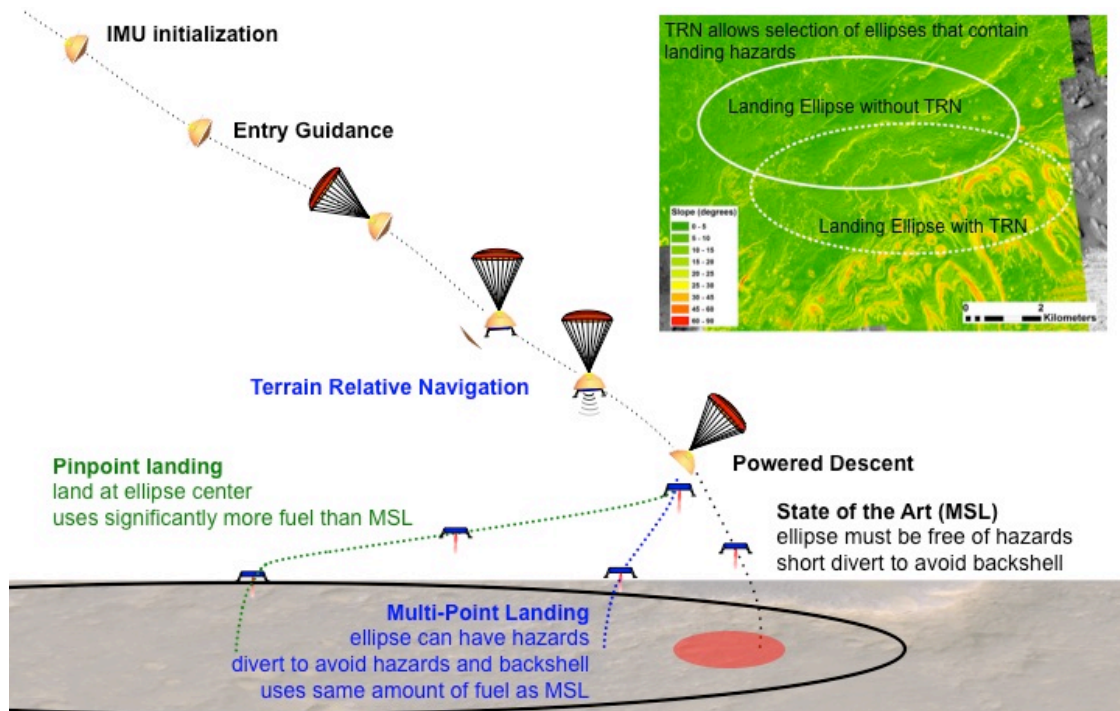


Figure 1. Next Generation Mars EDL capabilities, including multi-point and pin-point landing (Image Source Ref. 1).



Figure 2. ADAPT installed on the Xombie VTVL rocket vehicle, on the ground (left) and in flight (right, image credit NASA Photo / Tom Tschida).

development and testing. Masten hosted the ADAPT payload onboard their XA-0.1-B “Xombie” reusable vertical take off and vertical landing (VTVL) launch vehicle, used for low speed and low altitude testing.<sup>3</sup> The near-term focus for ADAPT was to mature and demonstrate two particular technologies developed at JPL: Guidance for Fuel-Optimal Large Diverts (G-FOLD), and the Lander Vision System (LVS), a smart sensor system for TRN. In 2012, during the first year of the ADAPT program, Xombie performed three envelope expansion flights to prove Xombie’s lateral divert capabilities and its ability to fly optimal trajectories computed by G-FOLD. These trajectories – position, velocity, and thrust as a function of time – were computed offline and stored in memory before launch. The three test flights culminated in a 750 m divert starting from an altitude of 430 m while descending vertically at 17 m/s.<sup>2,4</sup> During the second year, the team conducted three successful test flights where G-FOLD ran in real time on the ADAPT payload computer onboard the rocket. In the final flight, G-FOLD computed a three-dimensional, 800 m divert with direction reversal starting at an altitude of 295 m while descending at 17 m/s and traversing at 7.5 m/s, which was subsequently tracked by Xombie with several-meter precision.<sup>5</sup> This paper reports on the third year of the ADAPT program, during which the LVS was integrated with G-FOLD in the ADAPT payload and tested onboard Xombie (see Fig. 2). In flight, LVS fused data from a camera and an inertial measurement unit (IMU) to compute a precise estimate of Xombie’s position without GPS, which was then used by G-FOLD to compute a divert to a pre-selected landing site. Even though the Xombie flight trajectory was a scaled version of a Martian descent (i.e., starting at 300 m altitude at 10 m/s vertical velocity, rather than at 3 km and 100 m/s), the timeline and relative scale change were identical, so that LVS has to compute a navigation solution in 10 s while descending a third of its altitude as it is designed to do on Mars. However, as a consequence of the lower altitude, the LVS estimation accuracy is roughly ten times better than that expected on Mars. Two successful test flights in December 2014 demonstrated real-time performance and proper interaction of LVS and G-FOLD as it would happen during an actual Mars descent, localizing Xombie with meter-level precision, and planning and safely executing a fuel-optimal 300m lateral divert.

Safe and precise spacecraft landing is an active area of research. Several approaches for passive and active optical spacecraft TRN have been developed and are at various levels of maturity.

APLNav, developed at the Johns Hopkins Applied Physics Laboratory for lunar precision landing, uses correlation-based feature matches between images from two cameras and rendered image patches from an onboard map. Following a loose-coupling paradigm, image matches are first used to estimate the camera position and attitude in an iterative least squares estimator, and the resulting inferred pose measurement is then combined in a navigation filter using an EKF. APLNav has been tested in simulation, using helicopter test data, and (in part) onboard the Mighty Eagle VTVL test vehicle.<sup>6</sup>

The European Small Integrated Navigator for PLanetary EXploration (SINPLEX)<sup>7</sup> fuses data from an IMU, a startracker, and image feature tracks in an EKF-based simultaneous localization and mapping (SLAM) framework. SINPLEX has been tested at the Testbed for Robotic Optical Navigation (TRON) built by the German Aerospace Center (DLR).<sup>8</sup>

The Landstel algorithm<sup>9</sup> uses feature matches between onboard images and a map, that are not found based on correlation but rather using a descriptor extracted from the spatial distribution of neighboring features in a local neighborhood. The global pose estimate by Landstel is then fused with visual odometry in a loosely integrated filter. The approach has been tested on simulated lunar landing scenarios.

Draper Laboratory has been developing the Terrain-Relative Navigation & Descent Imager (TRNDI) add-on module for their GENIE Autonomous-GNC system.<sup>10</sup> TRNDI includes TRN, visual odometry, and hazard detection, as well as the GENIE Initial Direction Enhancer (GIDE) used to initialize heading. The integrated TRNDI/GENIE payload is planned to be tested within the Flight Opportunities Program, in a similar fashion as the ADAPT payload.

Johnson and Ivanov present results from an active optical, Light Detection and Ranging (LIDAR)-based TRN approach, that uses contour matching between lidar scans and a digital elevation map. Results from offline processing of helicopter field test data show position estimation accuracy of less than 90 m.<sup>11</sup>

Finally, the ALHAT project has been developing and flight testing precision landing sensors and hazard detection and avoidance (HDA) technology.<sup>12,13,14</sup> Ongoing work is focusing on integrating the navigation Doppler LIDAR sensor developed by the NASA Langley Research Center under ALHAT<sup>15</sup> with the ADAPT payload. Adding HDA functionality, i.e., mapping and analyzing surface terrain during descent to avoid landing on rocks or craters, could be considered in the future.

The remainder of the paper is organized as follows. After describing the Concept of Operations in Sec. II, we will focus on the algorithms (Sec. III), the avionics (Sec. IV), and the test vehicle (Sec. V), before reporting

the setup and results from the flight tests in Sec. VI. A summary in Sec. VII concludes the paper.

## II. Concept of Operations

The overall concept of an ADAPT test flight was to fly Xombie on a trajectory to set up (scaled) conditions of a Martian descent, trigger and initialize LVS at 300 m altitude, after 10 s hand the converged LVS solution to G-FOLD to compute a divert trajectory to a pad 300 m to the east, transfer this trajectory to the vehicle, and then follow this new trajectory to the ground (see Fig. 3). Early in the ADAPT payload design the question arose whether the error and latency of the Xombie navigation solution, particularly for attitude, was sufficiently small to meet the LVS initialization requirements. To mitigate this risk, the Poste Initialization and Propagation (PIP) system was added to the ADAPT payload. PIP computes the payload position, attitude, and IMU biases on the ground based on camera images of surveyed targets, and propagates the solution during vehicle ascent using the onboard IMU until TRN initialization. PIP and LVS together thus form a completely self-contained navigation solution, independent of the vehicle navigation system. PIP mirrors the functionality and error profile of the spacecraft GN&C system during Mars Entry, Descent and Landing, which is typically also based on IMU propagation. These systems both provide a highly accurate initial navigation state (except for a potentially km-level horizontal position error) to LVS.

Adding PIP and LVS to the ADAPT payload led to the need for increased visibility into and control over the payload prior to launch, resulting in the creation of a remote ground station that was able to communicate with the payload via a dedicated wireless connection. The ground station team was able to receive telemetry, re-configure system parameters, and start and stop the software, all while coordinating via radio with the MSS launch conductor. This capability proved vital to adapt to changing lighting conditions during the test campaign, monitor system health prior to liftoff, and also for system debugging, all without requiring physical proximity to a fueled and potentially pressured rocket. Throughout software operation, raw sensor data and software data products were logged onboard the payload on a solid state drive. In addition, telemetry was logged at the ground station. However, due to the geometry of ground station location and the trajectory profile, intermittent data drop outs in flight were expected, and hence the stored ground telemetry was only planned as a back-up.

On a typical test, PIP would compute an initial payload position and orientation estimate and report the results and intermediate data products (images, detected features, residuals) back to the ground station for evaluation and final parameter updates. The system was restarted, and a new solution for pose and IMU biases was obtained. From this point on, the system operated completely autonomously. Seconds prior to engine ignition, a Xombie mode transition triggered PIP to start propagating its pose using the ADAPT IMU data. The vehicle would rise vertically to 325 m altitude before settling in a 10 m/s constant velocity vertical descent. In case the vehicle does not receive a new trajectory from the ADAPT payload, or that trajectory is rejected for any reason, it would continue on this pre-loaded trajectory to land back on the launch pad. When the trigger conditions ( $302.5 \text{ m} \geq \text{alt} \geq 297.5 \text{ m}$ ,  $v_{\text{up}} \leq -9.0 \text{ m/s}$ ) were met, LVS was initialized using the propagated PIP pose and started estimating payload state using IMU data and camera observations. After 9.8 s (to account for 200 ms of average latency), LVS was queried for its current state estimate, and this estimate reported to G-FOLD 10 s after LVS initialization. As a bonus objective, LVS continued to operate after this point throughout the remainder of the flight. G-FOLD used the LVS position solution to compute a divert trajectory to a nominal target point 20 m above the center of the 300 m pad to the East, from which the MSS autoland guidance takes over until touchdown. For safety reasons, Xombie navigated using its GPS-INS navigation system throughout the flight. To avoid a discontinuity in the trajectory due to the LVS error that could result in a large response transient or even trigger an abort, G-FOLD based its trajectory starting point on the vehicle GPS-INS solution instead of the LVS solution. However, it computed the difference in horizontal position between the vehicle GPS-INS and the LVS solutions, and shifted its final target location by that amount, thus mimicking the behavior had the vehicle been navigated by LVS (a position estimation error would manifest as a landing error). The LVS horizontal position difference compared to Xombie’s navigation state had to be less than 10 m radial in order to be accepted by G-FOLD.

To accommodate the G-FOLD computation and trajectory transfer time, G-FOLD predicted the vehicle state 1 s forward using a constant velocity assumption and used that as the trajectory starting point. It then computed the fuel-optimal divert trajectory and transmitted it to the Xombie flight management system. The vehicle conducted its own acceptance tests, spliced the trajectory into its preloaded “launch-and-return”

trajectory, and started to track the new path. At the target location, MSS autoland guidance took control of the vehicle, compensated for the TRN error, and guided the vehicle to a safe landing on the pad center.

ADAPT software automatically shutdown when detecting a vehicle landing mode transition. Once the wireless connection was successfully re-established after touchdown, ground operators could safely power off the ADAPT payload remotely.

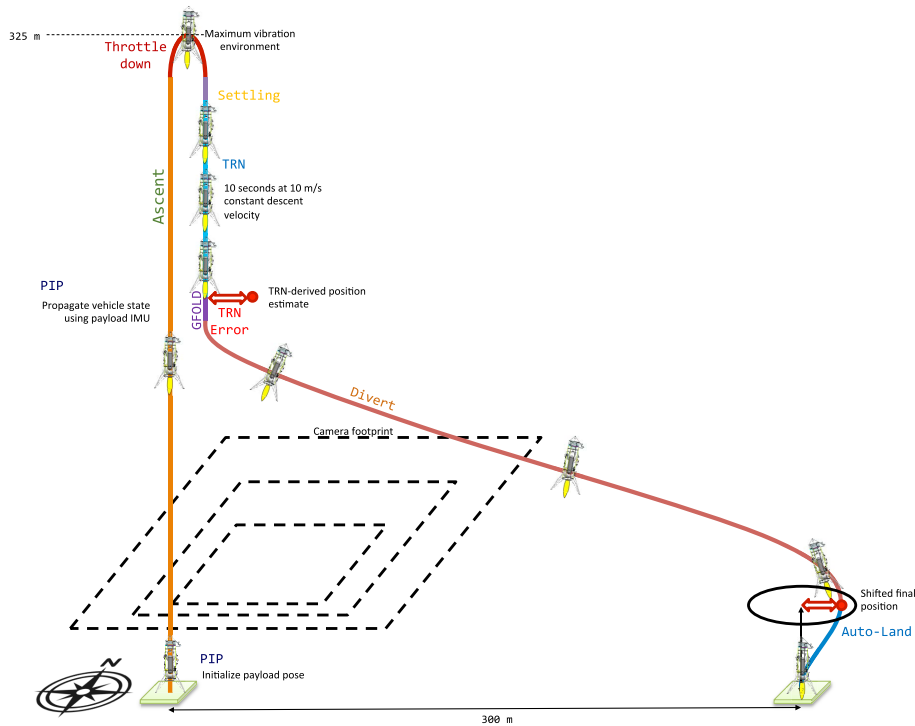


Figure 3. Concept of Operations for the ADAPT test flight on MSS's Xombie vehicle.

### III. Algorithms

#### A. Pose Initialization and Propagation

PIP determines the ADAPT payload position and attitude, as well as the ADAPT IMU biases on the ground, and then propagates that solution during Xombie's ascent to initialize LVS once the LVS trigger conditions are met. For the initial pose estimate, PIP uses camera observations of six surveyed ground targets, consisting of concentric contrasting circles.<sup>16,17,18</sup> The center location of each of the six circles is determined in the ECEF reference frame by using a total station to measure their position relative to three surveyed GPS reference markers with 12 m baseline, and then uploaded in the PIP parameter file. Once an image is taken, the image processing module detects and identifies the concentric contrasting circles and the pixel location of their centers. A sample output image with the overlaid ellipses is shown in Figure 4. This figure shows that this algorithm is robust to low levels of contrast, shadows and clutter. The center pixel coordinates, along with their surveyed Earth-centered Earth-fixed (ECEF) locations are used in a globally convergent algorithm to estimate the camera position and attitude.<sup>19,16,17,18</sup> The IMU biases can now be estimated by subtracting the expected gravity and earth rate signal, transformed into the IMU frame, from IMU measurements taken while the vehicle is stationary and averaged over four minutes. The IMU biases are assumed to be static over the time from PIP completion to LVS initialization. Shortly before lift-off, PIP is transitioned to propagation mode and starts integrating the IMU measurements using the computed initial pose estimate and biases,<sup>20,21,22</sup> and transfers this solution to LVS once the vehicle reaches the trigger conditions at 300 m altitude, typically after 50-60 s.

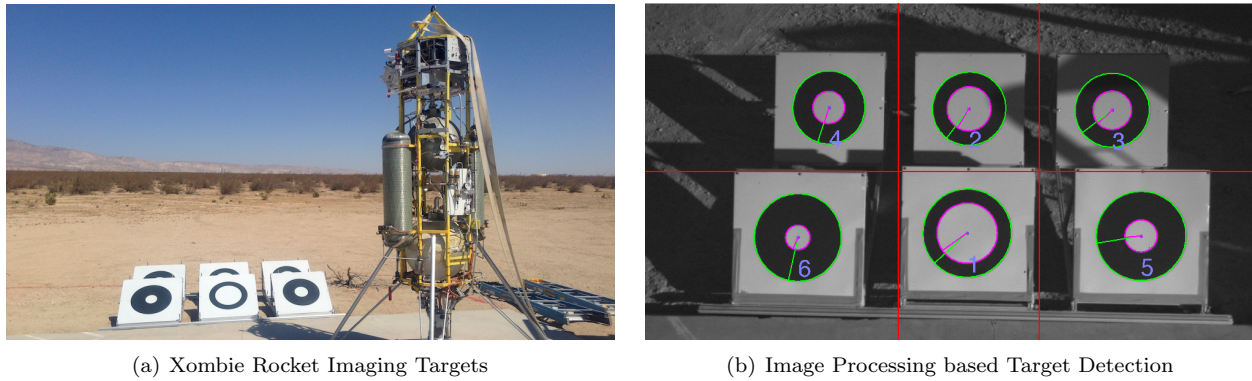


Figure 4. The Pose Initialization and Propagation (PIP) System

## B. Terrain-Relative Navigation

The LVS provides terrain-relative navigation by combining information from an IMU, a camera, and an onboard prior 3D terrain map.<sup>23</sup> To accommodate both large initial position error and provide high-accuracy pose estimates, TRN has a coarse and a fine navigation mode (see Fig. 5). For the first three images, three large image patches per image are matched to the map using frequency based correlation, allowing a large search area (left of Fig. 6). All nine of these matches are input at once into a batch estimator that combines them with IMU data to coarsely estimate position. This batch estimator updates the epoch state estimate valid at the time of TRN initialization using two nonlinear least squares iterations and re-integrates the trajectory. This batch estimator is designed to reduce km-level horizontal position error to less than 100 m on Mars, assuming attitude, velocity, and altitude are relatively well known from the onboard propagated IMU solution and an altimeter. Note that for the ADAPT tests, due to the short open-loop propagation time, the altitude error at LVS initialization was small enough so an altimeter was not necessary. Coarse navigation mode is followed by a refinement mode where, for each image, up to 256 small image patches are matched by spatial correlation to the map (right of Fig. 6), exploiting smaller image search areas enabled by the updated horizontal position estimate from the batch estimator. Of these, at most 100 are fused with IMU data in an extended Kalman filter (EKF)<sup>24,25</sup> that reduces the position estimate down to a few tens of meters. TRN can process images at approximately 1 Hz. Robust statistics are used throughout the image matching process to eliminate outliers that could cause large position errors. Image processing delays are addressed via state augmentation.<sup>24</sup>

In order for image processing to work properly, the error at TRN initialization was required to be within 12 m in altitude and  $2^\circ$  in heading (roll). In order to avoid imaging areas outside of the map, the vehicle roll angle was constrained to within  $\pm 5^\circ$  during the first 10 s of TRN operation. The horizontal position error between TRN and the vehicle GPS/INS solution had to be within 10 m at the time of G-FOLD initialization. All requirements were met in flight.

## C. G-FOLD

The problem of powered descent guidance is to determine a fuel optimal trajectory to a given target location that respects the vehicle’s dynamics and constraints, for example, maximum and minimum thrust, maximum speed, maximum thrust-angle-from-vertical, minimum glideslope constraints that prevent subsurface flight, or maximum change in thrust acceleration between time steps. It is these constraints that make polynomial descent guidance challenging.<sup>26</sup> To date, landers on the Moon and Mars have generally used variations on polynomial guidance or propellant-efficient gravity-turn guidance, neither of which explicitly enforced constraint satisfaction.<sup>5</sup> Whereas polynomial powered descent guidance is computationally efficient and sufficient for small diverts, G-FOLD solves for a globally fuel-optimal, constrained divert.<sup>27,26</sup> This is possible, since the constrained problem for a given time-of-flight was theoretically shown to be a convex optimization problem “in disguise”,<sup>28</sup> specifically a Second Order Cone Program (SOCP).<sup>29</sup> Such convex problems can be efficiently solved for a globally optimal trajectory using interior point methods (IPMs).<sup>30</sup> The optimal time-of-flight is then determined using a scalar line search optimization.

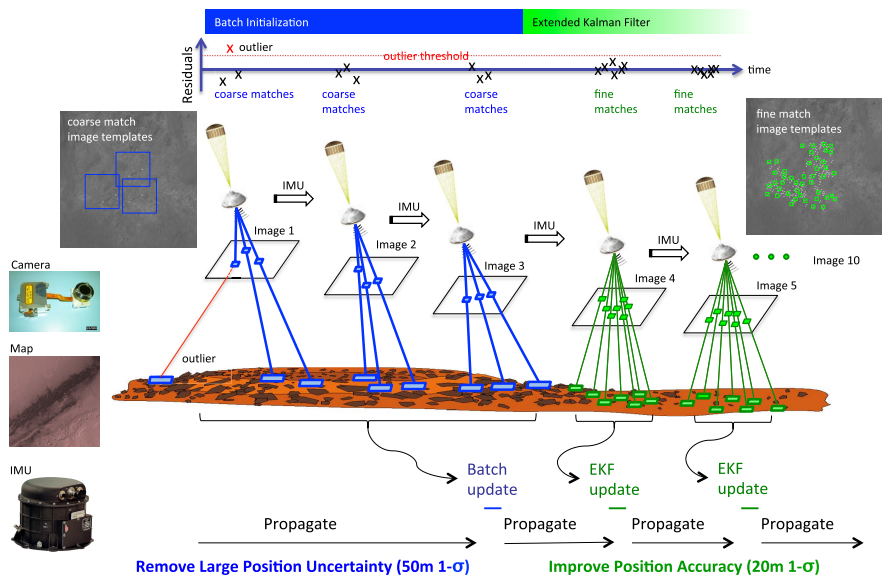


Figure 5. The LVS matches features from a camera against an onboard map and fuses them with IMU measurements. In a two-stage process, large position errors are first compensated using batch processing of three images, followed by precision pose estimation using an extended Kalman filter.

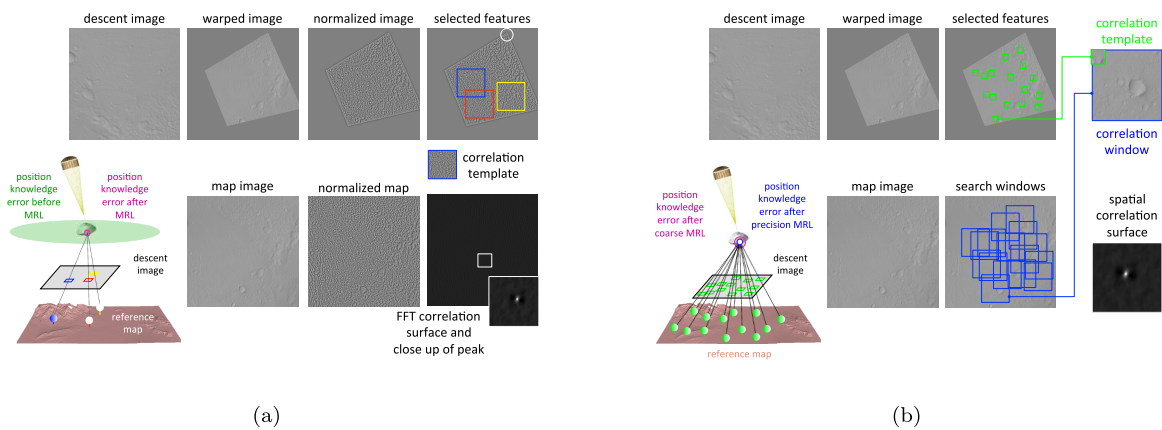


Figure 6. TRN image processing first removes large position uncertainty using frequency based correlation of a few landmarks (a) and then improves accuracy using spatial correlation of many landmarks (b).

G-FOLD consists of three principal components: 1) a time-of-flight optimizer that finds the optimal duration of a divert, 2) a parser that for a given time-of-flight puts the physical divert problem and its associated data in the standard mathematical form of an SOCP, and 3) a solver, customized for the ADAPT program at the University of Texas, that then finds optimal solution variables utilizing an IPM. The time-of-flight optimizer makes multiple calls to the parser/solver to find the divert duration the time-of-flight that minimizes to a specified tolerance.<sup>5</sup>

Two additional, application-specific components of G-FOLD are the state predictor and the trajectory table generator. The state predictor utilizes the expected vehicle dynamics during G-FOLD calculation to predict the state beyond the calculation lag of G-FOLD. This predicted state is then used as the initial condition for the divert trajectory. The trajectory table generator takes the discretized trajectory produced by parser and solver and turns in into a reference trajectory at the 50 Hz control rate of the vehicle. This reference trajectory is then transferred to the Xombie flight management system.

All three algorithms were running onboard the ADAPT payload, which is described next.

## IV. Avionics

The ADAPT payload was developed for flight in the payload bay at the top of the Masten Xombie vehicle and consists of two main assemblies – the payload assembly and the sensor assembly (see Fig. 7). A schematic view of the ADAPT payload is shown in Fig. 9.

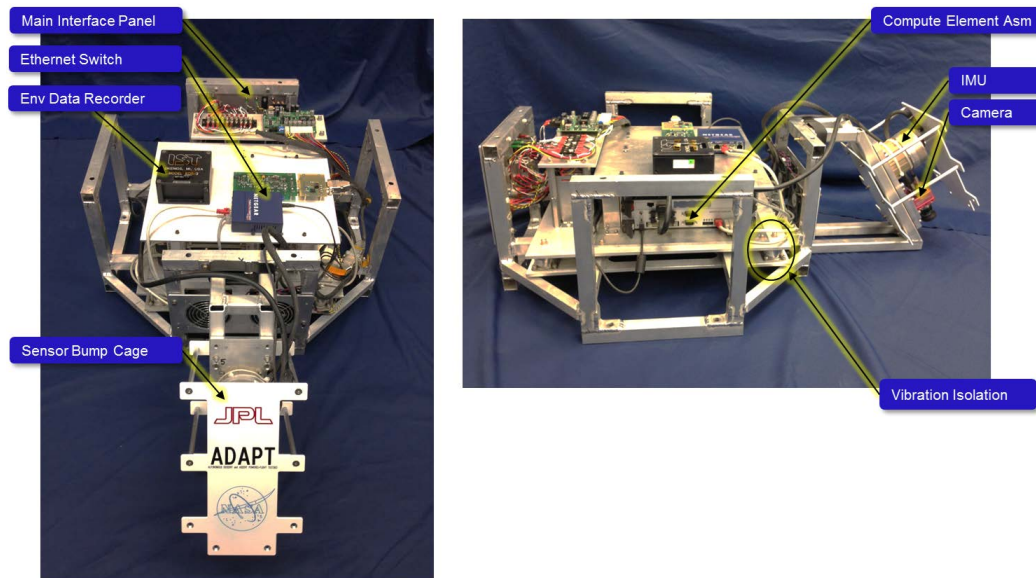


Figure 7. ADAPT Payload and Sensor Assembly.

### A. Payload Assembly

The ADAPT payload assembly consists of a compactPCI based compute assembly, batteries and power distribution, an Ethernet switch, wireless radio, and an environmental data recorder. The ADAPT compute assembly provides both LVS and G-FOLD functionality within a single 5-slot 6U compactPCI custom card cage. The LVS compute element is a hybrid processing system using an Aeroflex LEON3 compactPCI development board, an Alpha-Data Virtex 5 field programmable gate array (FPGA), and a custom sensor interface board. The FPGA board captures and time-stamps camera and IMU data in addition to performing all the image processing algorithms. The LEON board controls the FPGA and coordinates the execution of the TRN and PIP algorithms. The G-FOLD compute element (SBC) is a commercially available high-performance single board computer with an Intel mobile quad core processor. The SBC executes the G-FOLD algorithm, maintains separate communication channels with Xombie and the remote ground station, and logs all test telemetry. The wireless radio is used to initialize the system and to monitor telemetry from a remote base station approximately 1 km from the launch pad. Inside the payload, the PCI backplane is

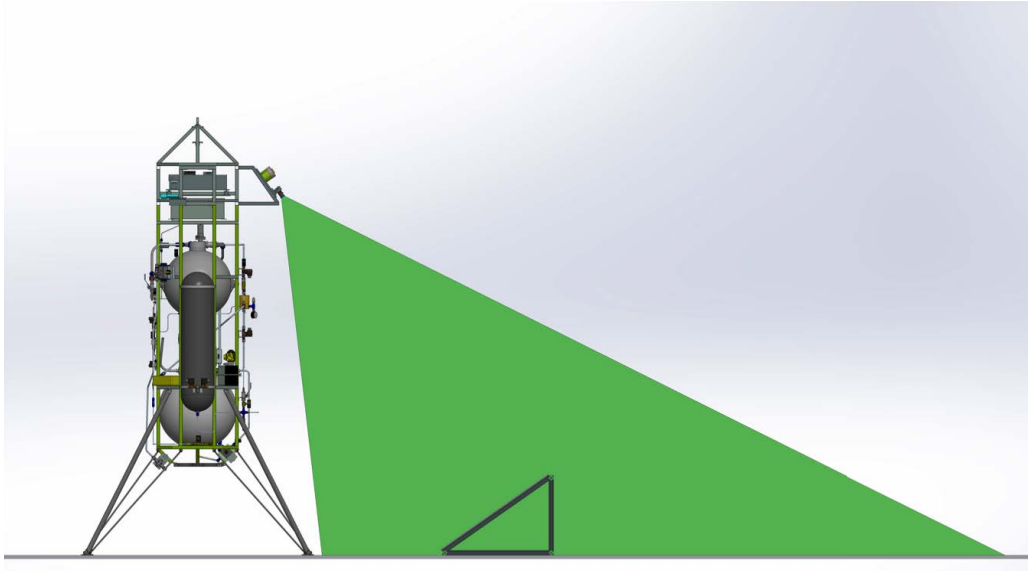


Figure 8. The ADAPT payload mounted on the top of MSS's Xombie VTVL vehicle.

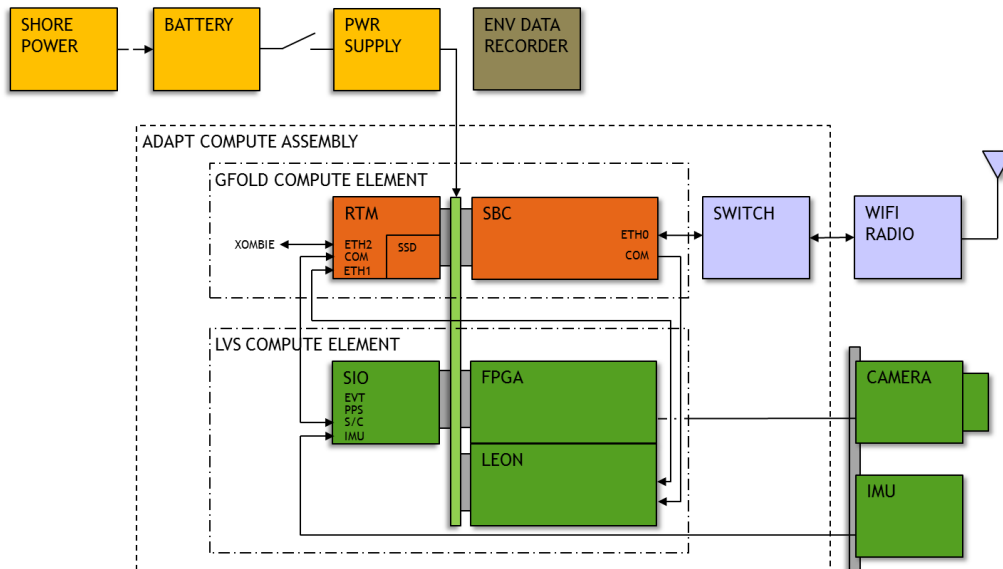


Figure 9. ADAPT Payload and Sensor Assembly Block Diagram.

used for transferring images and log files. TCP and UDP packets over a dedicated 100Base-T Ethernet link are used between the LEON and the SBC for commanding and telemetry. A rear transition module (RTM) provides additional interfaces and hosts the Solid State Drive (SSD) used for onboard data logging. The SBC uses another dedicated Ethernet port to communicate with the vehicle. This link is used to continuously receiving 50 Hz vehicle navigation state updates and sending 50 Hz G-FOLD state updates, as well as for transferring the G-FOLD trajectory to the vehicle. Loose time synchronization between LEON/FPGA, SBC, and vehicle is achieved by comparing send/receive network packet timestamps, under assumption of negligible network delay. The payload assembly is enclosed to reduce potential electromagnetic interference and to provide environmental (dust and moisture) protection. Isolators are used between the ADAPT payload assembly and the payload frame of the Xombie vehicle to reduce vibration and shock to the payload during transportation, flight, and landing. A self-contained environmental data recorder from Instrumented Sensor Technology with a three-axis accelerometer time tags all acceleration events to provide a history of the dynamic environment experienced by the payload during a flight.

## B. Sensor Assembly

The ADAPT sensor assembly consists of a Northrup Grumman LN200 inertial measurement unit (IMU) and a visible wavelength monochrome camera rigidly mounted to a baseplate. The camera is a global shutter  $1024 \times 1024$  pixel CMOS monochrome camera with camera link interface. A Schneider ruggedized C-mount lens with a  $60^\circ$  field-of-view is used. To have a clear view of the terrain below, the sensor assembly is mounted outside the payload frame and looks  $35^\circ$  off-nadir (see Fig. 8). A bump cage protects the sensor assembly from accidental contact and doubles as a sunshade.

## V. XA-0.1-B “Xombie” Test Vehicle

The Masten Space Systems XA-0.1-B “Xombie” is a reusable vertical take off and vertical landing (VTVL) launch vehicle used for low speed and low altitude testing (see Fig. 2). After placing in the 2009 Lunar Lander Challenge (a part of the NASA Centennial Challenges Program), the vehicle has served as a test platform for experimental spacecraft landing systems as a commercially-available lander testbed.<sup>3</sup>

The XA-0.1-B weighs approximately 176 kg, plus 130 kg of fuel. Xombie has a single engine, which can be gimballed independently in two directions up to  $8^\circ$  from the centerline. This engine has a thrust range of 1115 N to 3718 N, with a maximum velocity of 26.8 m/s in any component. The XA-0.1-B has been used to simulate both lunar and Martian landing profiles and is capable of high speed descent rates that are not achievable through conventional flight test platforms.

Xombie uses a combination of differential GPS and IMUs to provide sub-centimeter positioning accuracy. Xombie offers 24 V (+/-2 V) @ 10 A power and 40 kg mass capacity to hosted payloads. During flight, Xombie provides estimated vehicle attitude, attitude rate and mass at 50 Hz to the ADAPT payload. Xombie employs a supervisory control architecture as a fault protection scheme to protect the vehicle. The supervisory control monitors the state of the vehicle and takes over if any of the state parameters exceeds pre-defined limits. This allows the hosted payload maximum access to controlling the vehicle while not allowing its commands to harm the vehicle.

## VI. Flight Test Results

The test campaign was comprised of a series of validation and testing steps, including simulation, component level testing, a helicopter test campaign to validate LVS performance over the MSS launch pad, ground ops tests to test and validate PIP and its integration into the pre-launch procedure, Processor-in-the-Loop testing with MSS flight software, and several tether tests, culminating in two free flights on 12/04/2014 and 12/09/2014. The only difference between the free flights was the handling of the LVS solution. In Freeflight 1, an open-loop test, the LVS solution and the horizontal difference to Xombie’s GPS solution were computed but ignored, so that G-FOLD planned the trajectory to a point above the pad center. This test flight demonstrated proper software execution, interaction, and relative timing, and verified that the propagated PIP solution and the final LVS position error met accuracy requirements. In Freeflight 2, the LVS error was added to the G-FOLD target position, and the MSS autoland guidance executed a small divert to ensure a safe vehicle landing on the pad center, see the trajectory in Fig. 11. The ADAPT payload performed

flawlessly in both flights, and the results were very repeatable.

For feature matching, ADAPT carried an onboard map, i.e., a  $1024 \times 1024$  pixel, 1 m/pixel, georeferenced, orthorectified image of the test site. This map was obtained by combining 0.5 m/pixel RapidEye imagery collected on 09/07/2013 from BlackBridge<sup>a</sup> and terrain elevation data from the USGS 1/3-Arc Second National Elevation Dataset<sup>b</sup>. The resolution of the map was chosen to maximize tolerance to off-nadir angle pointing and initial estimation error while minimizing the scale difference between map pixel size and expected ground sample distance of the image footprints. The camera exposure time was set to 0.3 ms for both flights, based on the exposure of the PIP image and the expected lighting conditions at launch time. An example of the feature matches obtained in flight between the descent images and the map is shown in Fig. 10.

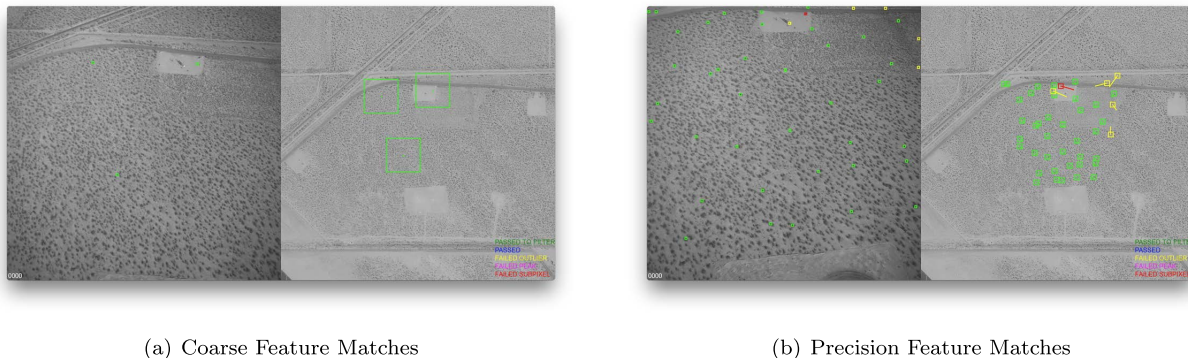


**Figure 10.** Example of LVS feature matches between a descent image (left) and the map (right) over the MSS test range during Freeflight 2. Features that are rejected as outliers are marked as red (failed subpixel interpolation) or yellow (failed geometric consistency check).

To compare ADAPT and Xombie navigation solutions, both had to be spatially aligned and time synchronized. Time alignment, as discussed previously, was based on packet receipt time, which did not account for network delays. Spatial alignment included the transform from ECEF to a surface-fixed East-North-Up (ENU) frame, and the transform from Xombie’s navigation body frame to the ADAPT IMU frame. Due to the absence of alignment features on the Xombie avionics, the Xombie to ADAPT body frame transformation was estimated based on technical drawings. The origin of Masten’s ENU navigation frame was fixed at zero at the actual launch position of the vehicle, which could vary between flights. Since the launch position of the vehicle was repeatable to within tens of centimeters, the ECEF-to-ENU transform was fixed based on the position of the Xombie IMU as estimated by PIP during tether test 5. This relatively loose alignment leads to some estimation bias, as evident in the estimation error plots in Fig. 12. Errors in the Xombie GPS-INS solution further contribute to the errors shown in Fig. 12, although these errors were assumed small due to MSS’s use of differentially corrected GPS. This is not the case for the initial heading (roll) estimate, which is poorly observable by GPS/INS while static, but converges during flight.

The PIP position error at LVS initialization was less than 2 m per axis and well within requirements. The attitude error was also well within requirements as evidenced from the minor attitude corrections after the start of the LVS fine navigation phase. Note that the attitude error compared to the vehicle attitude solution, as plotted in Fig. 12, is a poor benchmark for validating attitude requirements due to the loose vehicle/payload alignment and the still-converging heading estimate. During the 10 s nominal LVS period of operation, LVS processed 10 images and successfully matched up to 49 features per image to the onboard map, allowing it to precisely estimate the rocket position, velocity, and attitude within the required time (see Fig. 13). The LVS horizontal position error compared to the Xombie GPS solution at handover to G-FOLD was less than 2 m per axis, and well within requirements ( $<10$  m). Bonus images were successfully processed and image matches generated for almost 20 s after the end of nominal LVS operations until at approximately 85 m altitude the scale difference precluded successful feature matching. This further demonstrates excellent robustness against scale mismatch between image and map. The estimation error remains stable after the last feature matches were generated. The coarse match estimate computed approximately 3 s after start

<sup>a</sup>[www.blackbridge.com](http://www.blackbridge.com)

<sup>b</sup>[http://nationalmap.gov/3dep\\_prodserv.html](http://nationalmap.gov/3dep_prodserv.html)

of LVS and corrected with the first precision match image 2 s later has considerably larger error than the precision match estimate, even though the prior estimate delivered by PIP is very well aligned with the fine match solution. This degraded accuracy after coarse match is partly expected due to the small number and lower matching precision of the coarse features but still came as a surprise, in particular since the magnitude and direction of the error was very consistent between the two flights. Ongoing analysis since the test flights has already identified and corrected some contributing error sources, such as small biases introduced during map generation and map cropping.

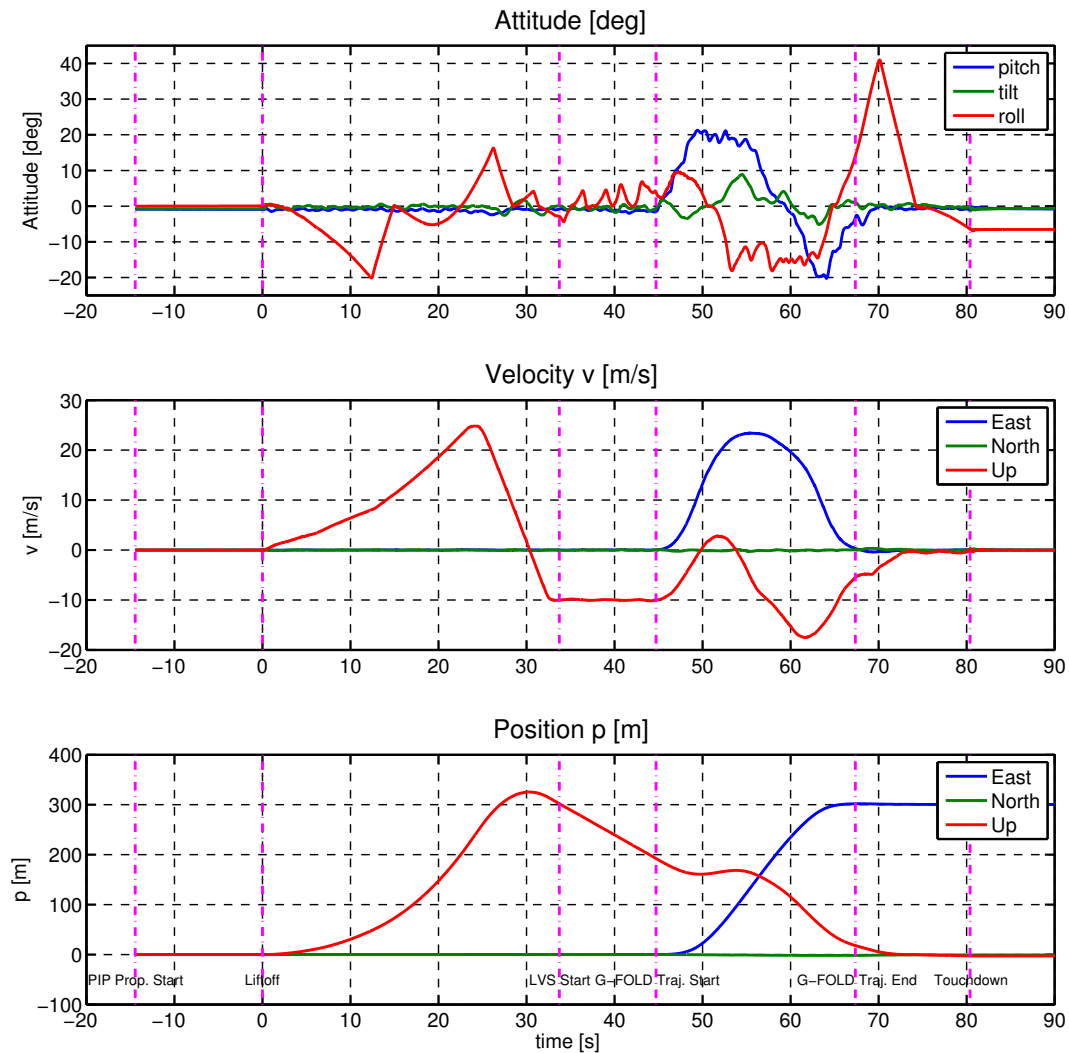


Figure 11. Xombie Freeflight 2 trajectory.

The metrics used to evaluate G-FOLD and Xombie performance are: position and velocity tracking errors, vehicle attitude during LVS operation, commanded trajectory discontinuities, commanded feedback acceleration, event timing analysis and fuel usage. Fig. 14 shows the 3D trajectory commanded and navigated. There are two visible discontinuities in the commanded trajectory at the start and end of the G-FOLD trajectory, also clearly visible in Fig. 15. The discontinuity at the beginning of the G-FOLD trajectory is due to the 1 s constant-velocity prediction of the vehicle state, which is used as the initial state for the G-FOLD trajectory computation. This discontinuity has a magnitude of 0.4 m in the vertical direction. The discontinuity at the G-FOLD trajectory end is due to the transition to the vehicle autoland mode, which

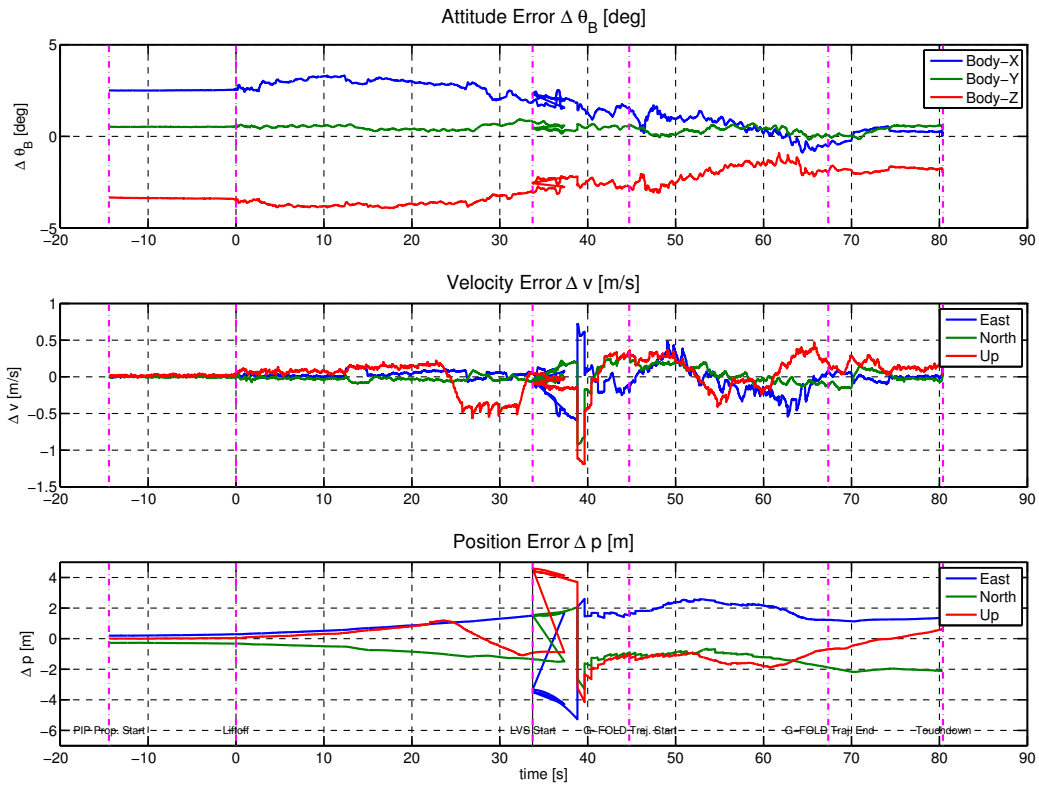


Figure 12. PIP and LVS Freeflight 2 estimation errors compared to Xombie's GPS-INS estimate. The horizontal position error at 43.5 s was used to compute the G-FOLD target location.

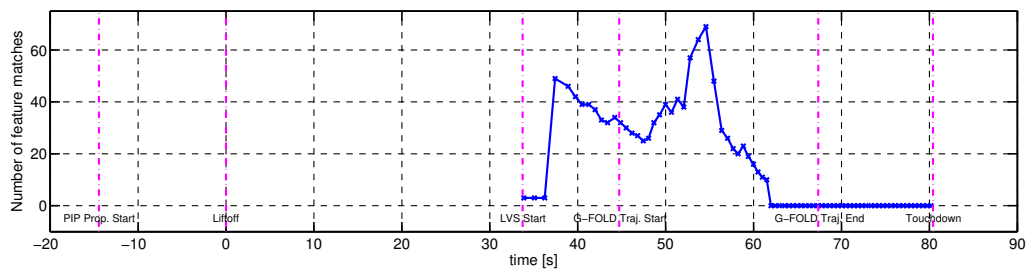


Figure 13. LVS feature matches during Freeflight 2.

switches the commanded state to one a few meters above the landing pad. This discontinuity is equal to the horizontal TRN error of  $\begin{bmatrix} 1.56 & -1.14 & 0 \end{bmatrix}$  m in ENU coordinates, determined 9.8 s after TRN initialization (see Fig. 12).

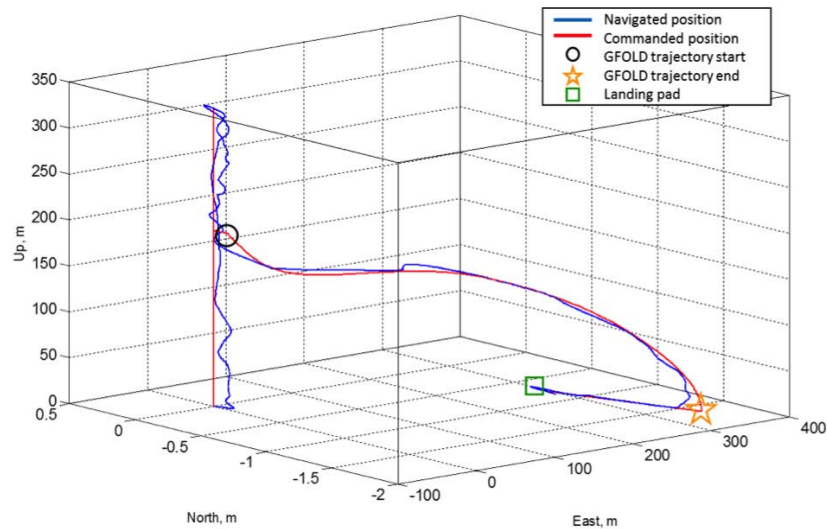


Figure 14. 3D commanded and navigated (actual) position of Xombie during Freeflight 2. Note the unequal scale in the North axis, exaggerated to show tracking performance and G-FOLD trajectory start and end points.

Velocity tracking was below 0.5 m/s throughout the trajectory, and the discontinuities are very small, which helps the position tracking performance.

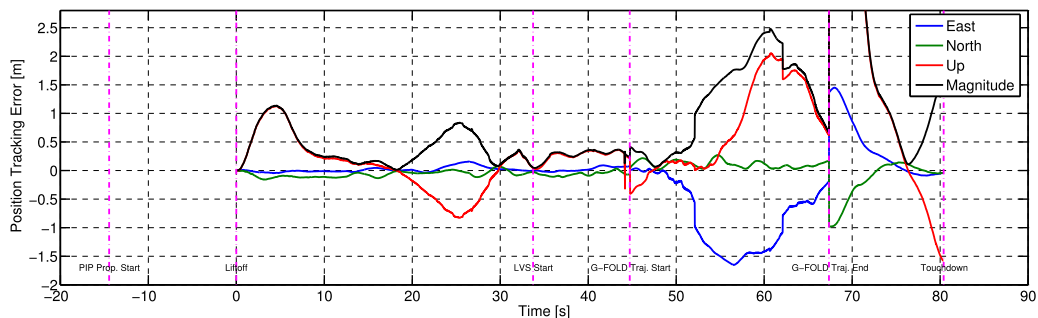


Figure 15. Freeflight 2 trajectory tracking error. Maximum error was 2.5 m during the lateral divert ( $\sim 60$  s), due primarily to aerodynamic drag acceleration pushing the vehicle up (red line) and uprange (blue line). The large discontinuity at G-FOLD trajectory end is due to the transition to autoland mode; the commanded position becomes the landing pad.

It was imperative that the vehicle keeps a constant attitude during the 10 s LVS operation phase in order to ensure that the camera images fall within the provided map, especially at the highest point, when the sensitivity of camera footprint location to attitude changes is greatest. Roll angle is controlled using deadbands, which were adjusted to provide a maximum expected roll angle of  $5^\circ$ . Although the roll angle surpassed the  $5^\circ$  constraint in two occasions, the events happened in the lower part of the LVS phase and all images were contained within the image map (see top of Fig. 11). The  $5^\circ$  roll angle deadbanding during TRN can be seen between 35 s and 45 s. When the lateral divert starts, the vehicle must pitch in the direction of the location of the landing pad in order to accelerate. Aerodynamic torques roll the vehicle as it accelerates starting at 50 s. To decelerate in preparation for landing, the vehicle must pitch in the direction opposite to its velocity, starting at 60 s. The roll angle goes back to zero once the lateral velocity and aero torques

decrease. After the transition to autoland mode the vehicle follows a different guidance scheme that allows for larger roll angles.

The maximum speed was constrained to 25 m/s in an effort to limit the aerodynamic forces acting on the vehicle. This was a proxy to ensure the feedback acceleration command was below a 4 m/s<sup>2</sup> constraint. The feedback acceleration command is added to the reference trajectory acceleration profile to compensate for, among other errors and uncertainties, the aerodynamic forces, which are not accounted for by G-FOLD. Reaching the limit feedback acceleration command would mean a sudden loss of trajectory tracking performance, which might lead to a trajectory abort if the errors become too large. The limit in feedback acceleration command is in place to ensure the safety of the vehicle. During the Freeflight 2 the feedback acceleration command did not exceed 2 m/s<sup>2</sup>. The total used fuel was 118 kg, leaving 18 kg of unused fuel. During the landing phase the fuel depletion rate is about 1 kg/s. The timing analysis shows that the TRN phase took 10.02 s from trigger to the time a solution was provided. A solution was requested after 9.8 s, indicating a 220 ms latency (typical 200 ms). G-FOLD computation time was 100 ms (typical 80 ms). Trajectory transfer to the vehicle took 60 ms (typical 60 ms). GFOLD computation and trajectory transfer delays are only a fraction of the 1 s slot provided. The total delay of the G-FOLD trajectory start compared with the expected was 260 ms: 220 ms from the TRN latency and 40 ms from a 2 RTI mismatch in the vehicle internal clocks due to flight management system overloading during G-FOLD trajectory transfer and splicing. The acceptable delay range was determined via simulation to be 100-400 ms.

## VII. Conclusion

In the third year of the ADAPT program, PIP, LVS and G-FOLD were integrated in the ADAPT payload, providing end-to-end precision pose initialization, terrain-relative navigation and optimal large-divert guidance capabilities. Two successful flights on 12/04/2014 and 12/09/2014 on the Masten XA-0.1-B “Xombie” VTVL rocket vehicle demonstrated a real-time, complete pin-point descent and landing system for planetary landers. This paper described the test flight concept of operations, the individual algorithms, the ADAPT avionics, and reported on the test flight results. Currently, work is underway to integrate the ADAPT payload with a navigation Doppler Lidar velocimeter, developed under the ALHAT program, to continue the maturation of future precision landing technology.

## Acknowledgments

This work was conducted at the Jet Propulsion Laboratory, California Institute of Technology, under contract with the National Aeronautics and Space Administration. NASA Flight Opportunities Program managed by NASA Armstrong Flight Research Center funded the test flights. Government sponsorship acknowledged.

## References

- <sup>1</sup>Johnson, A. E., Cheng, Y., Montgomery, J. F., Trawny, N., Tweddle, B., and Zheng, J. X., “Real-Time Terrain Relative Navigation Test Results from a Relevant Environment for Mars Landing,” *Proc. AIAA Guidance, Navigation, and Control Conference*, Kissimmee, FL, Jan. 05 - 09, 2015.
- <sup>2</sup>Aung, M., Açıkmese, B., Johnson, A., Regehr, M., Casoliva, J., Mohan, S., Wolf, A., Scharf, D., Ansari, H., Masten, D., Scotkin, J., and Nietfeld, S., “ADAPT – A closed-loop testbed for next-generation EDL GN&C systems,” *Proc. 36th AAS Guidance & Control Conference*, Breckenridge, CO, Feb. 3–6, 2013.
- <sup>3</sup>Frampton, R. V., Ball, J., Masten, D., Ferguson, P., Oittinen, K. C., and Ake, C., “Planetary Lander Testbed for Technology Demonstration,” *Proc. AIAA SPACE 2013 Conference and Exposition*, Sept. 2013.
- <sup>4</sup>Açıkmese, B., Aung, M., Casoliva, J., Mohan, S., Johnson, A., and Scharf, D. P., “Flight Testing of Trajectories Computed by G-FOLD: Fuel Optimal Large Divert Guidance Algorithm for Planetary Landing,” *Proc. 23rd AAS/AIAA Spaceflight Mechanics Meeting*, Kauai, HI, 2013.
- <sup>5</sup>Scharf, D. P., Regehr, M., Dueri, D., Açıkmese, B., Vaughan, G., Benito, J., Ansari, H., Aung, M., Johnson, A., Masten, D., Nietfeld, S., Casoliva, J., and Mohan, S., “ADAPT Demonstrations of Onboard Large-Divert Guidance with a VTVL Rocket,” *Proc. IEEE Aerospace Conference*, Big Sky, MT, 2014.
- <sup>6</sup>McGee, T. G., Rosendall, P. E., Hill, A., Shyong, W. J., Criss, T. B., Reed, C., Chavers, G., Hannan, M., Epp, C., and Nishant, M., “APLNav: Development Status of an Onboard Passive Optical Terrain Relative Navigation System,” *Proc. AIAA Guidance, Navigation, and Control Conference*, Kissimmee, FL, Jan. 05–09, 2015.
- <sup>7</sup>Steffes, S., Dumke, M., Heise, D., Sagliano, M., Samaan, M., Theil, S., Boslooper, E., Oosterling, H., Schulte, J., Skaborn, D., Söderholm, S., Conticello, S., Esposito, M., Yanson, Y., Monna, B., Stelwagen, F., and Visee, R., “Target relative navigation

results from hardware-in-the-loop tests using the SINPLEX navigation system,” *Proc. 37th Annual AAS Guidance and Control Conference*, No. AAS 14-402, Breckenridge, CO, Feb. 2014.

<sup>8</sup>Krüger, H., Theil, S., Sagliano, M., and Hartkopf, S., “On-ground testing optical navigation systems for exploration missions,” *Proc. 9th ESA Conference on Guidance, Navigation & Control Systems*, Porto, Portugal, June 2–6, 2014.

<sup>9</sup>Van Pham, B., Lacroix, S., and Devy, M., “Vision-based Absolute Navigation for Descent and Landing,” *J. Field Robot.*, Vol. 29, No. 4, July 2012, pp. 627–647.

<sup>10</sup>Steiner, T. and Brady, T., “Vision-based navigation and hazard detection for terrestrial rocket approach and landing,” *Proc. IEEE Aerospace Conference*, March 2014, pp. 1–8.

<sup>11</sup>Johnson, A. and Ivanov, T., “Analysis and Testing of a LIDAR-Based Approach to Terrain Relative Navigation for Precise Lunar Landing,” *Proc. AIAA Guidance, Navigation, and Control Conference*, Aug. 2011.

<sup>12</sup>Epp, C., Robertson, E., and Carson, J. M., “Developing Autonomous Precision Landing and Hazard Avoidance Technology from Concepts through Terrestrially Flight-Tested Prototypes,” *Proc. AIAA Guidance, Navigation, and Control Conference*, January 05–09, 2015.

<sup>13</sup>Trawny, N., Huertas, A., Luna, M. E., Villalpando, C. Y., Martin, K., Carson, J. M., Johnson, A. E., Restrepo, C., and Roback, V. E., “Flight testing a Real-Time Hazard Detection System for Safe Lunar Landing on the Rocket-Powered Morpheus Vehicle,” *Proc. AIAA Guidance, Navigation, and Control Conference*, January 05–09, 2015.

<sup>14</sup>Amzajerdian, F., Pierrottet, D. F., Hines, G. D., Roback, V. E., Petway, L. B., Barnes, B. W., Brewster, P. F., and Bulyshev, A. E., “Advancing Lidar Sensors Technologies for Next Generation Landing Missions,” *Proc. AIAA Guidance, Navigation, and Control Conference*, January 05–09, 2015.

<sup>15</sup>Pierrottet, D. F., Amzajerdian, F., Petway, L. B., Hines, G. D., and Barnes, B., “Field Demonstration of a Precision Navigation Lidar System for Space Vehicles,” *Proc. AIAA Guidance, Navigation, and Control (GNC) Conference*, Aug. 2013.

<sup>16</sup>Tweddle, B. E. and Saenz-Otero, A., “Relative Computer Vision-Based Navigation for Small Inspection Spacecraft,” *Journal of Guidance, Control, and Dynamics*, 2014/11/06 2014, pp. 1–9.

<sup>17</sup>Tweddle, B., “Relative Computer Vision Based Navigation for Small Inspection Spacecraft,” *Proc. AIAA Guidance, Navigation, and Control Conference*, Aug. 2011.

<sup>18</sup>Tweddle, B. E., *Computer Vision Based Navigation for Spacecraft Proximity Operations*, Master’s thesis, Massachusetts Institute of Technology, USA, 2010.

<sup>19</sup>Haralick, R. M., Joo, H., Lee, C., Zhuang, X., Vaidya, V. G., and Kim, M. B., “Pose Estimation from Corresponding Point Data,” *IEEE Transactions on Systems, Man and Cybernetics*, Vol. 19, No. 6, 1989, pp. 1426–1446.

<sup>20</sup>Bortz, J., “A New Mathematical Formulation for Strapdown Inertial Navigation,” *IEEE Transactions on Aerospace and Electronic Systems*, Vol. AES-7, No. 1, Jan. 1971, pp. 61–66.

<sup>21</sup>Savage, P. G., “Strapdown Inertial Navigation Integration Algorithm Design Part 2: Velocity and Position Algorithms,” *Journal of Guidance, Control, and Dynamics*, Vol. 21, No. 2, March – April 1998, pp. 208–221.

<sup>22</sup>Savage, P. G., “A Unified Mathematical Framework for Strapdown Algorithm Design,” *Journal of Guidance, Control, and Dynamics*, Vol. 29, No. 2, March – April 2006, pp. 237–249.

<sup>23</sup>Johnson, A., Bergh, C., Cheng, Y., Clouse, D., Gostelow, K., Ishikawa, K., Katake, A., Klaasen, K., Mandic, M., Morales, M., Park, S., Sirota, A., Spiers, G., Trawny, N., Waters, J., Wolf, A., Zheng, J., and Zheng, W., “Design and Ground Test Results for the Lander Vision System,” *Proc. AAS GN&C Conference*, Breckenridge, CO, 2013.

<sup>24</sup>Trawny, N., Mourikis, A. I., Roumeliotis, S. I., Johnson, A. E., and Montgomery, J. F., “Vision-aided Inertial Navigation for Pin-Point Landing using Observations of Mapped Landmarks,” *Journal of Field Robotics*, Vol. 24, No. 5, May 2007, pp. 357–378.

<sup>25</sup>Mourikis, A., Trawny, N., Roumeliotis, S., Johnson, A., Ansar, A., and Matthies, L., “Vision-Aided Inertial Navigation for Spacecraft Entry, Descent, and Landing,” *IEEE Transactions on Robotics*, Vol. 25, No. 2, April 2009, pp. 264–280.

<sup>26</sup>Steinfeldt, B., Grant, M., Matz, D., and Braun, R., “Guidance, Navigation, and Control System Performance Trades for Mars Pinpoint Landing,” *AIAA Journal of Spacecraft and Rockets*, Vol. 47, No. 1, 2010.

<sup>27</sup>Ploen, S., Açikmeşe, A., and Wolf, A., “A Comparison of Powered Descent Guidance Laws for Mars Pinpoint Landing,” *Proc. AIAA/AAS Astrodynamics Specialist Conference*, 2006.

<sup>28</sup>Açikmeşe, B. and Ploen, S. R., “A convex programming approach to constrained powered descent guidance for Mars pinpoint landing,” *AIAA Journal of Guidance, Control, and Dynamics*, Vol. 30, No. 5, 2007.

<sup>29</sup>Boyd, S. and Vandenberghe, L., *Convex Optimization*, Cambridge University Press, New York, NY, 2004.

<sup>30</sup>Peng, J., Roos, C., and Terlaky, T., “Primal-Dual Interior-Point Methods for Second-Order Conic Optimization Based on Self-Regular Proximities,” *SIAM Journal on Optimization*, Vol. 13, No. 1, 2002.